ELSEVIER

Coordination Chemistry Reviews 228 (2002) 1–18

COORDINATION CHEMISTRY REVIEWS

www.elsevier.com/locate/ccr

Paramagnetic spectroscopy of vanadyl complexes and its applications to biological systems

Thomas S. Smith II [a,b], Russell LoBrutto [a,b,*], Vincent L. Pecoraro [a,b,*]

[a] *Department of Chemistry, The University of Michigan, 930 North University Avenue, Ann Arbor, MI 48109-1055, USA*
[b] *Department of Plant Biology, The Center for the Study of Early Events in Photosynthesis, Arizona State University, Tempe, AZ 85827-1601, USA*

Received 14 November 2000; received in revised form 18 July 2001; accepted 21 September 2001

Contents

Abstract

The ability to determine the ligand environment around vanadium(IV), usually as the vanadyl ion (VO^{2+}), has become crucial to the understanding of many biological systems. In addition to those systems in which vanadium naturally occurs, the vanadyl ion has found favor as a spectroscopic probe in place of spectroscopically silent cations, EPR, ESEEM, and ENDOR spectroscopies are the tools of choice for examining these paramagnetic systems. A variety of model complex studies allow good comparisons to be made to known vanadium environments. The complimentary nature of the strengths and weaknesses of these techniques can combine to give an accurate picture of the metal ligation in a number of cases herein. © 2002 Published by Elsevier Science B.V.

Keywords: Vanadium; Vanadyl; Electron paramagnetic resonance spectroscopy; Electron spin echo envelope modulation spectroscopy; Electron-nuclear double resonance spectroscopy

* Corresponding authors. Tel.: +1-743-763-1519; fax: +1-313-647-4865.
E-mail address: vlpec@umich.edu (V.L. Pecoraro).

0010-8545/02/$ - see front matter © 2002 Published by Elsevier Science B.V.
PII: S0010-8545(01)00437-4

1. Introduction

The study of the chemistry of vanadium has been driven by its presence in biological systems. Although, vanadium's existence in ascidians was discovered in 1911 by Henze [1], the vast majority of work has occurred more recently. Vanadium is now known to occur naturally in mushrooms as well, and is required as an essential cofactor in certain haloperoxidases and nitrogenases [2]. While vanadium is suspected to be an essential trace element for humans [3], as vanandate, it is known to affect phosphate metabolism and various forms of vanadium have proven to have insulin-mimetic effects [4]. The ability to substitute vanadyl ion for spectroscopically silent divalent cations, such as Mg^{2+}, Ca^{2+}, and Zn^{2+} has led to the increased use of vanadyl ion (VO^{2+}), as a spectroscopic probe of biological systems using paramagnetic spectroscopic techniques, such as electron paramagnetic resonance (EPR), electron spin echo envelope modulation (ESEEM), and ENDOR. These techniques can provide information as to the number, kinds and in some cases, orientations of ligands around the metal binding site.

The intent of this paper is twofold. First, it is a compilation of recent work involving paramagnetic spectroscopy of the vanadyl ion in various complexes and biomolecules. Particular attention is paid to advances that have shown what the spectroscopic methods are, and are not capable of examining. Work since the Eaton and Eaton review (1990) will be emphasized [5]. Other reviews since 1990 by Makinen and Mustafi [6] and by Chasteen [7] are recommended. Second, it is also meant to act as a beginning resource to those who may be interested in starting to use vanadyl ion as a spectroscopic probe in their own system. Since, detailed descriptions of the theoretical basis of these spectroscopic techniques are covered in several books and articles, only a brief introduction is given to familiarize those, who may not have used these techniques before. However, the reader should obtain a clear sense of the scope of each technique sufficient to pursue work in more detail.

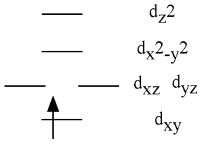

Fig. 1. Orbital energy levels for the d electrons of the vanadyl ion (VO^{2+}).

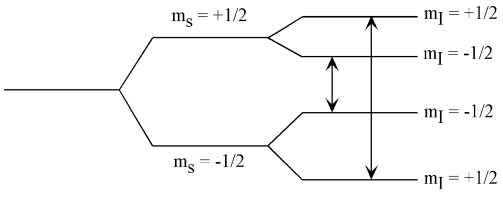

Fig. 2. The spin state transitions observed in the EPR are shown here for a system with both electron spin $S = 1/2$ and nuclear spin $I = 1/2$.

While there are examples of non-oxo vanadium(IV) complexes in nature, such as amavadin, the oxophilicity of vanadium(IV) causes the overwhelming majority of vanadium(IV) compounds to contain the vanadyl ion [8,9]. Vanadyl ion does oxidize in aerobic aqueous solution, but at such a slow rate that it can generally be dismissed as negligible. The $+4$ oxidation level can be stabilized by the addition of other ligands or reducing agents. Vanadyl complexes, typically adopt 5-coordinate square pyramidal or 6-coordinate distorted octahedral, geometries, with the vanadium–oxo distance (ca. 1.6 Å) being shorter than the distance from the metal to the ligand *trans* to the oxo (ca.2–2.2 Å). Vanadium(IV) has a d^1 electron configuration. A d orbital energy level diagram for the vanadyl ion is shown in Fig. 1. The lone d electron is in a σ-nonbonding orbital, which points away from the ligands in the *xy* plane. These characteristics will be important in the discussions to follow.

2. Electron paramagnetic resonance (EPR)

2.1. Introduction to technique

The underlying theory behind EPR can be found in any number of textbooks, including ones by Drago [10], Abragam [11], and more recently, Solomon and Lever [12]. EPR spectroscopy examines the transitions between electron spin states separated by the presence of an external magnetic field. These states are separated by an energy dependent on the g value of the observed species (for the theoretical 'free' electron, $g = 2.0023$) and the magnetic field applied, as shown in Fig. 2. Values of g in vanadyl EPR spectra are typically less than the free electron value, usually ca.1.95. The transition is induced by microwave radiation of frequency ν, such that $h\nu = g\beta H$, where h is Planck's constant, β is the Bohr magneton, and H is the magnitude of the applied field. Note that unlike NMR, in the EPR experiment, the frequency is held constant, and it is the strength of the magnetic field, which is varied. These electronic states are then split by their interaction with the spin of the nucleus—termed hyperfine coupling. For the case of vanadium(IV), the nuclear spin of ^{51}V is $I = 7/2$, so the states are split into $2I + 1 = 8$ different energy states each, separated by the hyperfine coupling constant, A. Almost all ($> 99\%$) vanadium is ^{51}V, so there are no additional isotopes with nuclear spin to complicate the spectrum. Further splitting of states by nearby nuclei, such as ^{14}N is referred to as superhyperfine coupling. For the vanadyl case, due to the

Table 1
Contribution to $A_{\parallel}$ of different binding moieties (in units of $\times 10^{-4}$ cm^{-1})

Binding group	$A_{\parallel}$ contribution	Reference
H_2O	45.7	[15]
Perp. imidazole =N–	45.5	[20]
Aliphatic imine =N–	44.4	[15]
Cl^-	44.1	[25]
Amide (DMF) HC(O)NRR′	43.7	[16]
RCO_2^-, $ArCO_2^-$	42.7	[15]
PO_4^{3-}	42.5	[75]
Pyridine =N–	40.3	[15]
RNH_2	40.1	[15]
Par. imidazole =N–	40	[20]
OH^-	38.7	[15]
ArO^-	38.6	[19]
acac, 1 O eq. =C–O$^-$	37.6	[19]
RO^-	35.3	[15]
ArS^-	35.3	[15]
Deprot. amide RC(O)NR′$^-$	30–32 (ligand charge −2); 37–43 (ligand charge −4)	[19,25]
RS^-	31.9	[15]

electron residing in a σ-non-bonding orbital pointing away from the ligands in the equatorial (xy) plane, superhyperfine coupling to nitrogen-containing ligands is not resolved in a typical X-band (9 GHz) EPR spectrum. Therefore, there is no additional splitting of the EPR absorption. EPR transitions are electronic in nature, and their selection rules can be expressed as $\Delta M_s = \pm 1$, $\Delta M_I = 0$, as shown in Fig. 2. For a vanadium(IV) complex, this gives rise to an eight-line spectrum.

Symmetry can also have an effect on EPR spectra. If the spectra are obtained from frozen solutions or as a powder, where the anisotropy is not averaged away by motion of the molecule, a complex pattern can emerge. For example, the electronic configuration around a metal ion may have a unique axis of symmetry. In the commonly employed first derivative display, two superimposed spectra with different hyperfine splittings will be obtained from frozen solutions ('axial symmetry'). If all three axes in the molecular frame of reference are electronically distinct, three different splittings may be obtained ('rhombic symmetry'). Due to the strong vanadium–oxygen interaction in the vanadyl unit, axial or nearly axial EPR spectra are usually observed for vanadyl complexes. The parallel transitions, (representing the orientation of the V=O bond parallel to the applied magnetic field), exhibit hyperfine coupling constants that are larger than those for the perpendicular orientation.

2.2. The additivity relationship

EPR spectroscopy is a powerful tool that provides information about the elemental composition, nuclearity, and electronic structure of a paramagnetic state. Typically, investigators determine the apparent g value to assess the spin state of a molecule. They can use the extent and magnitude of hyperfine coupling to identify the nuclei to which the unpaired electron(s) are coupled and to determine the number of nuclei associated with an EPR transition. Through variable temperature and power studies, one can extract great detail about the electronic structure of a paramagnetic ion. The strength of vanadium(IV) is in its use as a probe of ligand environment. Since, the ion has a simple $S = 1/2$ electronic spin, and because, ^{51}V has high natural abundance and an $I = 7/2$ nuclear spin, the vanadyl ion can be used to assess the bonding of ligands to the divalent complex ion. An additivity relationship, first proposed by Wuthrich [14] and refined later by Chasteen [15], allows the hyperfine coupling constant, specifically $A_{\parallel}$, to be correlated to the number and types of ligands present in the equatorial plane. This theory has evolved from merely correlating the isotropic hyperfine coupling constant, A_o ($A_o = [A_{\parallel} + 2A_{\perp}]/3$), with the number of nitrogens and oxygens in the equatorial plane to extracting $A_{\parallel}$ values and using these hyperfine constants as more sensitive probe of electronic environment. Each ligand has a specific contribution to $A_{\parallel}$, and the sum of the four equatorial ligands' contributions will give the $A_{\parallel}$ observed. Examination of Table 1 reveals that the contribution to $A_{\parallel}$ correlates approximately inversely with the electron donor capacity of the ligand, with the most donating ligands contributing the least to the hyperfine coupling. The typical $A_{\parallel}$ varies between 31.9×10^{-4} and 45.7×10^{-4} cm^{-1}, with the generally accepted error being ca. $\pm 1.5 \times 10^{-4}$ cm^{-1} [15]. This introduces one caveat into the use of the additivity relationship, there is often more than one combination of ligands which can, within the error limits, give the experimentally determined $A_{\parallel}$. Therefore, one must either know which types of ligands are possible (as in the case of small molecules with previously characterized ligands), or use other complementary techniques to narrow down the possibilities.

Both the older additivity method using A_o and the newer method using $A_{\parallel}$ continue to be used in the literature. Unfortunately, many authors only report one or the other hyperfine coupling value. Results using the different approaches cannot be compared directly as $A_{\perp}$ is not known. A proper analysis requires that A_o be converted to $A_{\parallel}$. As $A_{\parallel}$ and $A_{\perp}$ can be obtained from an EPR spectrum with equal ease, it is preferable to list all values of the hyperfine coupling to facilitate comparison of results. Also for ease of comparison, values should be reported in units of 10^{-4} cm^{-1} or MHz, not

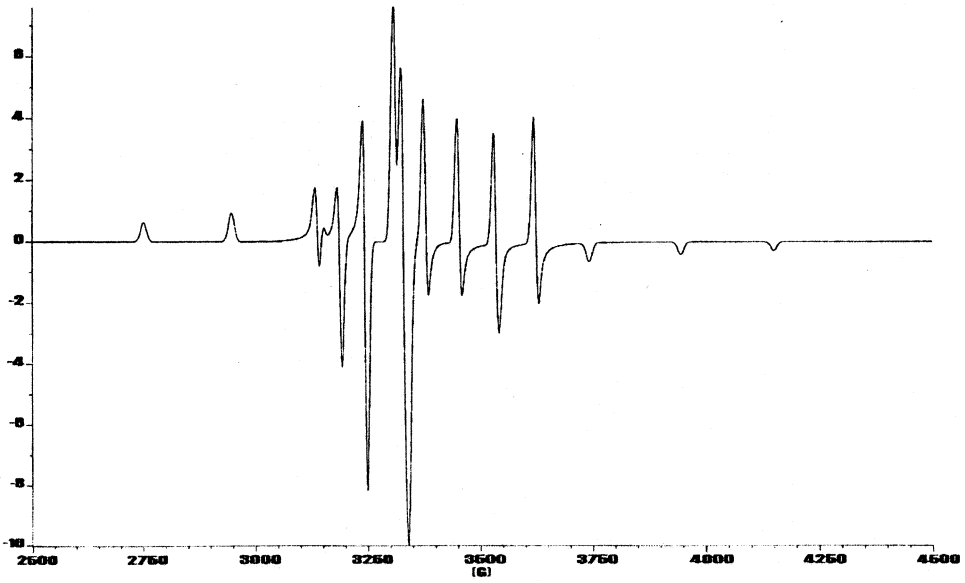

Fig. 3. A hypothetical vanadyl EPR spectrum shown as the first derivative spectrum with the SIMFONIA software by Bruker Instruments, Inc [13].

as hyperfine splittings, (in units of Gauss or Tesla),which are still dependent on the g value.

The following is an example of the approach using the EPR spectrum shown as Fig. 3. The parallel lines, exhibiting the widest splitting, are the lines of interest. First, $g_{\|}$ must be determined, using the formula $hv = g\beta H$. The field values should be referenced to an external sample such as diphenylpicrylhydrazyl (DPPH), and if possible, the precise frequency of the instrument should be monitored with a frequency counter. The value for the magnetic field is obtained by averaging the field values of the two outermost lines. Then to obtain $A_{\|}$, the separation between the two outermost lines is divided by seven. The individual separations between lines are not exactly equal, but they average out to the appropriate value [15]. Since, this $A_{\|}$ value is in terms of magnetic field and dependent on the g value, it is multiplied by the previously obtained value of $g_{\|}$ and also by the Bohr magneton to convert the value into wavenumbers. This number can be used with Table 1 to show that the equatorial ligands in this case are some combination of waters, or perpendicularly oriented imidazoles. These g and A values should then be confirmed by computer simulation with software such as QPOW [17] or SIMFONIA [13] as the instructions outlined above do not include second order corrections.

2.3. Model complexes

Recently, a surprising amount of work with model complexes has served to refine the additivity relationship with regard to ligand orientation. Cornman and co-workers have found changes to the hyperfine coupling constant with the degree of distortion, τ, (Fig. 4) of five-coordinate vanadyl complexes. Using phenolate and imine ligands exclusively, as the complexes' geometry distorted more towards trigonal bipyramidal, the total $A_{\|}$ for the complexes dropped from 161.7×10^{-4} to 157.3×10^{-4} cm^{-1} [18]. Cornman's group also noticed a wide range of values, when extracting the contribution to $A_{\|}$ of a coordinated deprotonated amide. Values from 31×10^{-4} to 37×10^{-4} cm^{-1} were observed [19].

Until very recently, the accepted $A_{\|}$ for imidazole coordinated to the vanadyl ion was tied to that used for pyridines and other 'aromatic imines' [18]. Smith et al. used six-coordinate complexes to demonstrate a change in the $A_{\|}$ contribution of imidazole ligands as the orientation relative to the vanadyl unit was systematically varied. The change was sizable, with an imidazole with its ring plane parallel to the vanadium–oxo vector having a contribution to $A_{\|}$ of ca. 40×10^{-4} cm^{-1} and one positioned perpendicular to the V=O, having a contribution of ca. 46×10^{-4} cm^{-1}. The dependence of the $A_{\|}$ contribution on angle is a function of $\sin(2\theta - 90)$, obtained from the crystallographically-characterized vanadyl complexes, shown in Fig. 5[20]. Since, there were only a few crystallographically char-

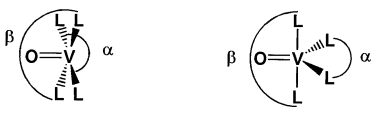

Fig. 4. The distortion parameter τ is defined in terms of the angles α and β as shown. $\tau = (\beta - \alpha)/60$, such that in the ideal square pyramid on the left, $\tau = 0$, and in the ideal trigonal bipyramid on the right, $\tau = 1$.

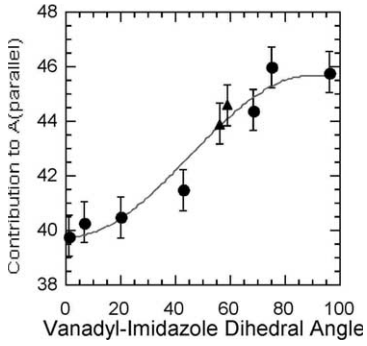

Fig. 5. Graph plotting the contribution to $A_{\|}$ by imidazole (in units of 10^{-4} cm^{-1}) vs. the angle made by the imidazole ring to the vanadyl unit. The curve fit is $A_{\|} = x + y\ \sin(2\theta - 90)(x = 42.722,\ y = 2.9638,\ R = 0.977)$. Reprinted with permission from [20]. Copyright 2000 American Chemical Society.

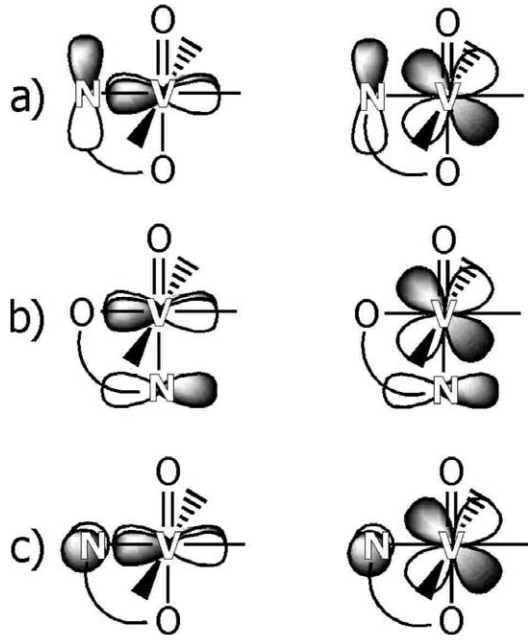

Fig. 6. Drawings of the overlap of the vanadyl d_{xy}, d_{xz}, and d_{yz} orbitals with the nitrogen p (aromatic) orbital from the imidazole. (a) The imidazole is bound in the equatorial position and in the perpendicular orientation. (b) The imidazole is bound in the axial position. (c) The imidazole is bound in the equatorial position and in the parallel orientation. Reprinted with permission from [20]. Copyright 2000 American Chemical Society.

acterized vanadyl imidazole complexes with which to calibrate this interaction, previous investigators had deduced the $A_{\|}$ for the most common (parallel) orientation, without recognizing the importance of ligand orientation.

These observations can be explained by considering the donation from ligand π orbitals to the metal ion. Fig. 6 uses the case with imidazole as an example. When the imidazole ring is perpendicular to the vanadyl unit, the aromatic p orbital on the nitrogen directly coordinated to the vanadium is parallel to the V=O unit. This would place it in position to overlap slightly with the d_{xz} or d_{yz} orbitals. Since, these orbitals are already participating in a strong bonding interaction with the vanadyl oxygen, this would be unfavorable. For the parallel ring case, however, the aromatic p orbital would overlap with the partially occupied σ-nonbonding d_{xy} orbital, and so would result in additional electron donation. This is consistent with the parallel imidazole having a lower contribution to $A_{\|}$. This effect seems to apply for non-aromatic imine ligands as well, and may be general to ligands containing perpendicular p donor orbitals.

In light of these results, previously reported data using vanadyl as a spectroscopic probe can be re-examined. While studying bovine carboxypeptidase A in 1974, Chasteen and co-workers substituted vanadyl ion for the active site zinc and observed values of $A_{\|}$ of 166.6×10^{-4} cm^{-1} at pH > 5 and 175.8×10^{-4} cm^{-1} below pH 5 [21]. The high pH form was initially assigned to an equatorial coordination of two imidazoles and two waters, and the low pH form, without a higher value known for imidazoles with a perpendicular orientation, was assigned to carboxylate coordination. However, the new values for imidazole suggest a coordination environment of [⊥ imidazole, ∥ imidazole, carboxylate, water] with a calculated $A_{\|}$ of 174.4×10^{-4} cm^{-1}. A ligand set for the higher pH form can be reached by deprotonating the water to give [⊥ imidazole, ∥ imidazole, carboxylate, hydroxide] with a calculated $A_{\|}$ of 167.4×10^{-4} cm^{-1}. Lipscomb and co-workers have since solved the X-ray structure of bovine carboxypeptidase A, and the ligands to the active site zinc are indeed water, carboxylate, and two imidazoles whose ring planes are at right angles to each other [22].

The EPR of the reduced vanadium bromoperoxidase can be reinterpreted as well. There are two published $A_{\|}$ values for reduced VbrPO—one at low pH ($A_{\|} = 166.6 \times 10^{-4}$ cm^{-1}), the other at high pH ($A_{\|} = 159.9 \times 10^{-4}$ cm^{-1}) [23]. The ligand set [⊥ imidazole, ∥ imidazole, alkoxide, hydroxide] gives a calculated $A_{\|} = 160.0 \times 10^{-4}$ cm^{-1}, well within allowable error for the high pH case [20]. For low pH, the ligand set [⊥ imidazole, ∥ imidazole, alkoxide, water] has a calculated $A_{\|} = 167.0 \times 10^{-4}$ cm^{-1}, which is also in very close agreement to the observed data. As the recently published crystal structure of the non-reduced vanadium bromoperoxidase shows three histidines and a serine near the active site, these ligand sets are reasonably possible [24].

A recent article [25] by Tasiopoulos et al. also shows a variation in deprotonated amide values, but over an even wider range than that observed by Cornman [19]. The contribution from deprotonated amide ligands was measured to be between 29 and 43×10^{-4} cm^{-1}. The authors attributed this wide variation to an effect of the

increasing negative charge of the donors in the equatorial plane; that is, an effect above and beyond the lowering of $A_{\|}$ by more donating ligands. When the charge of the donating ligands changed from -2 to -4, the additivity contribution from the deprotonated amide ligand increased by 5×10^{-4} cm^{-1}. The authors also noticed that the value in five coordinate complexes was lower than six coordinate complexes by about 5×10^{-4} cm^{-1}, which is evidence that the distortion to a square pyramidal or trigonal bipyramidal geometry is affecting the observed number.

Hagen and co-workers have studied a series of vanadyl bis(phenolate) complexes with varying substituents on the aromatic rings [26]. They observed that the HOMO–LUMO transitions, oxidation potentials, and EPR hyperfine couplings for these complexes obey linear relationships dependent on the Hammett constants of the aromatic ring functionalization. Different substituents on the aromatic ring of the ligand varied A_{iso} by up to 0.7 G. The electronic differences caused by the changing substituent could be a contributor to the causes of error in the additivity relationship, since the values used for a particular binding group do not take into account differences in the ligand as a whole.

Mondal and co-workers have synthesized a vanadium(IV/V) mixed valent dimer, that typifies the use of EPR to determine electronic communication [27]. The dimer consists of two ligands (deprotonated salicylaldimine of L-alanine) attached to a $V_2O_3^{2+}$ core. The bridging oxygen–vanadium bond lengths in the core are different by ca. 0.2 Å, signifying that the complex is essentially valence localized. In EPR spectra of the powder and frozen solutions, a typical eight-line axial spectrum is seen that confirms this assignment. However, in a room temperature (r.t.) solution sample in dichloromethane, a 15-line spectrum is seen, showing the vanadium dimer, is best described as a class II mixed valence complex (Fig. 7).

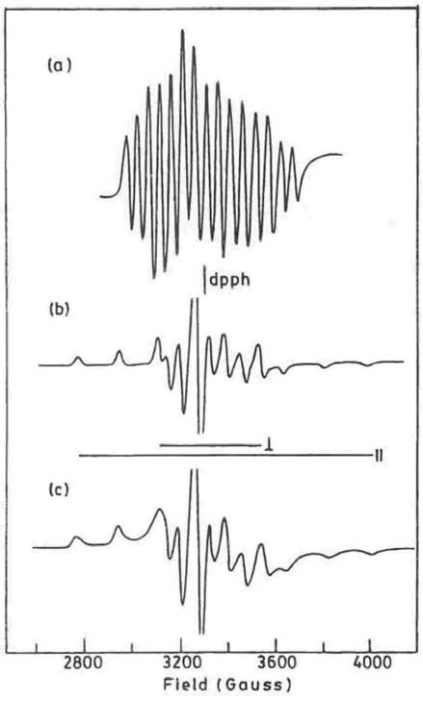

Fig. 7. EPR spectra of the complex $[Et_4N][V_2O_3(L\text{-alsal})_2]$ under the following conditions: (a) solution at 300 K; (b) solution at 77 K; (c) powdered solid at 300 K. Reprinted with permission from [27]. Copyright 2000 American Chemical Society.

EPR and the additivity relationship have been used to confirm the structures of many vanadyl complexes, including those with salicylaldehyde–amino acid Schiff base ligands [28], insulin-mimetic dithiocarbamate complexes [29], two binding sites on tetracycline [30], and aspartic acid complexes [31]. Amin and co-workers tracked by EPR the formation of different isomers of the insulin-mimetic complex $VO(H_2O)(acac)_2$ in vivo [32]. EPR has also been used to confirm the equivalence of the two metal centers in a ferromagnetically coupled vanadium(IV/IV) dimer [33]. Dessi, Micera, and Sanna catalogued the EPR data for a very large number of complexes with small biological molecules such as glycine, cysteine, cysteamine, and glutathione [34]. Jiang and Makinen, as well as Micera et al. have studied vanadyl's interaction with guanosine 5′-monophosphate [35,36].

2.4. Biological systems

Vanadium substitution of the active site metals in enzymes can be a highly informative method for determining the binding residues involved. In order to be certain that the vanadyl ion is binding to the same residues as the native metal, additional tests should be performed. These should include kinetic studies with the vanadyl-substituted enzyme to make sure that it retains appreciable activity compared with the native form. Confirming that the vanadyl-substituted enzyme retains its native structure and responds to any known inhibitors also serves to verify vanadyl coordination at the appropriate site. The reader should bear these precautions in mind while reading the following sections.

Werneberg and Ash used EPR to study vanadyl-substituted pyruvate carboxylase [37]. The vanadyl-substituted enzyme was found to have 30% of the activity of native enzyme, but only functioned in the reverse reaction (the native enzyme is capable of catalysis in either direction). They found two binding sites—one protein-dependent and one nucleotide-dependent. The nucleotide-dependent one, which formed upon addition of ATP, has an $A_{\|} = 176.4 \times 10^{-4}$ cm^{-1}. From this it was concluded that the equatorial ligand set for this vanadium consists of two phosphates and two waters, with a calculated $A_{\|} = 176.8 \times 10^{-4}$ cm^{-1}. For the protein site, $A_{\|} = 163.1 \times 10^{-4}$ cm^{-1}. Further, evidence was

accumulated by using D_2O to exchange away protons on ligands such as water or the lysine amine side chain. This will narrow the linewidths in the EPR spectrum by ca. 0.75×10^{-4} cm^{-1} per ligand [38]. A narrowing of 1.6×10^{-4} cm^{-1} was observed, giving two ligands with two exchangeable protons each. One possible ligand set would then be two (primary) amines, one parallel imidazole, and one carboxylate, yielding a calculated $A_{\parallel} = 162.9 \times 10^{-4}$ cm^{-1}. Bicarbonate added to the system, induced a drop in $A_{\parallel}$ of 4.3×10^{-4} cm^{-1}, but the exact cause of this cannot be determined. Werneberg and Ash also used thallous ion to study the relationship of the vanadyl site to a known nearby monovalent cation binding site. Superhyperfine coupling with Tl^{+} can be observed in vanadyl EPR, and the superhyperfine coupling is different for the parallel lines than for the perpendicular if the coupling is through space rather than through bond [39]. In this case, the couplings were equal, so Tl^{+} and VO^{2+} share a common ligand.

Hanson, Sun, and Orvig have used EPR to determine the nature of the insulin-mimetic complex bis(maltolato)-oxovanadium(IV) in solution [40]. Since there is no established additivity relationship contribution for maltolato-type ligands, different equatorial ligand environments could not simply be deduced from the observed hyperfine coupling. However, the general trends therein allowed *cis* coordination of solvents such as pyridine and water to be determined.

Hu and co-workers have used vanadyl ion as a spectroscopic probe in their studies of a mutant of the chloroplast F_1-ATPase. Vanadyl ion was found to serve as a functional co-factor for the enzyme. To determine, whether the glutamic acid to glutamine mutation was of a residue that served as a ligand, vanadyl ion was placed in the metal binding site of both the wild type and mutant proteins. Since, the change of a carboxylate to either a water or an amide would result in a change in $A_{\parallel}$, the EPR would be able to indicate whether the mutation affected metal binding. No changes were observed in the EPR spectrum, suggesting that the changed carboxylate was not involved [41].

Chen, LoBrutto, and Frasch have combined EPR with site-directed mutations in the vanadyl-substituted chloroplast F_1-ATPase, to provide proof of a specific residue binding to vanadium [42]. By replacing a threonine postulated to be binding to vanadium, the $A_{\parallel}$ values were altered drastically. With the cysteine mutation, the ligand set shifted from two alkoxides, a phenolate, and a carboxylate/phosphate to thiolate, phenolate, and two carboxylates/phosphates. The aspartic acid mutation caused a severe coordination change for which the only reasonable ligand set was alkoxide, phenolate, and two amines. Finally, mutation of the threonine residue to the hydrophobic leucine resulted in the almost total disappearance of the spectrum—the vanadium no longer bound to the enzyme, which precluded any of the above mutation effects from being merely a change in metal binding site.

The Frasch group also mutated a residue thought to be involved in metal binding site in the latent form of chloroplast F_1-ATPase [43]. The original site has been assigned an equatorial ligand set for vanadyl of two carboxylates/phosphates, alkoxide, and water. The residue changed this time was an aspartic acid. A change to histidine altered the hyperfine coupling so that the ligand set derived from the additivity relationship was parallel imidazole, carboxylate/phosphate, alkoxide, and water—apparently a simple substitution. A threonine mutation did not result in a simple substitution, but produced a change in ligand set to amine, phenolate, carboxylate/phosphate, and water. This change is reasonable, given a known nearby lysine and tyrosine. Asparagine and cysteine mutations apparently had no effect on the EPR spectrum, but a change from an amide to a carboxylate/phosphate would give a very small difference to $A_{\parallel}$. Similarly, the difference between carboxylate/phosphate + alkoxide and thiolate + water is also too small to observe reliably.

2.5. Caveats

Although, it is a very powerful method for determining ligands in the equatorial plane of vanadyl complexes, EPR is not a stand-alone identification technique. There is a small range of hyperfine coupling constant values given the relatively large error (ca. 1.5×10^{-4} cm^{-1}) involved in the additivity relationship. Care must be taken in applying the additivity relationship. In some cases, multiple, chemically reasonable fits to hypothetical ligand sets are possible, all of which may be within the error limits of the additivity calculation. Here are a few examples.

Kiss and co-workers have identified speciation between vanadyl bis(picolinate) complexes and vanadyl complexes with one picolinate and one citrate ligand [44]. However, since both ligands contain carboxylate, and their reported hyperfine coupling values for the complexes are only 1×10^{-4} cm^{-1} apart, this cannot be confirmed. Other examples where statistically insignificant differences between alternative coordination sphere formulations are available. These include attempts to distinguish between phosphate and carboxylate coordination [45] and perpendicular imidazole and water coordination [46] with only EPR as characterization.

Another example where allowable experimental error needs to be considered is Ceccato and co-worker's model complex for vanadyl-transferrin with phenolate, amine, and carboxylate ligation. Although, the A_o values for the two systems are close together (92.97×10^{-4} cm^{-1} for the model complex, 93.7×10^{-4} cm^{-1} for vanadyl-transferrin), the $A_{\parallel}$ values are outside the

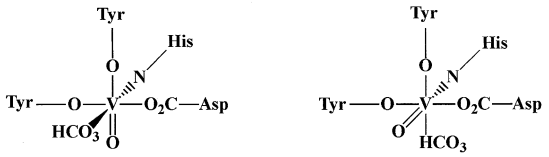

Fig. 8. Possible binding modes for vanadyl to transferrin. Tyrosine, histidine, aspartate, and bicarbonate make up the equatorial ligands for the mode on the left with the vanadyl unit pointed down. On the right, two tyrosines, aspartate, and bicarbonate are bound equatorially with the vanadyl unit coming out of the page.

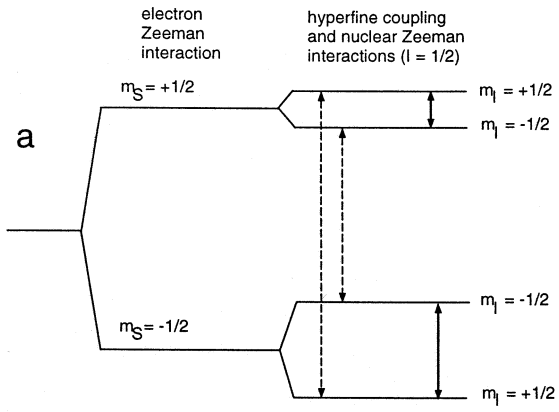

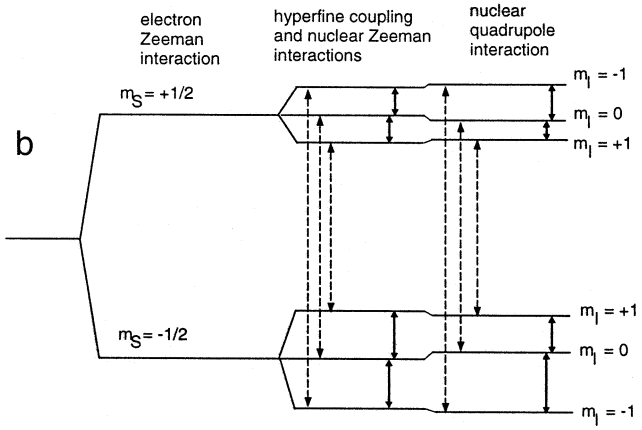

Fig. 9. EPR (dashed lines) and ENDOR (solid lines) spin transitions for $S = 1/2$ system, with hyperfine coupling to a nucleus with, (a) $I = 1/2$; and (b) $I = 1$; the effect of the nuclear quadrupole coupling is illustrated on the right hand side of diagram (b).

accepted error range (164.5×10^{-4} cm^{-1} for the model complex, 168×10^{-4} cm^{-1} for vanadyl-transferrin) [47]. Fig. 8 shows the two most logical coordination spheres for vanadyl ion at the active site of transferrin. In the first case, the ligand set of [two phenolates, carboxylate, bicarbonate] gives a calculated $A_{\|} = 162.6 \times 10^{-4}$ cm^{-1}, which is not similar to the observed value (assuming bicarbonate's contribution to $A_{\|}$ is similar to carboxylate's). The second possible ligand set [phenolate, perpendicular imidazole, carboxylate, bicarbonate] gives a much closer value for $A_{\|}$ of 169.4×10^{-4} cm^{-1}. Additional evidence from ESEEM and ENDOR (vide infra) upholds this conclusion.

2.6. Summary of EPR capabilities

To date, interpretation of the EPR spectra of vanadyl complexes is unique in that it can be directly correlated to the equatorial ligand types. By determining the parallel hyperfine coupling constant and comparing it to published values for ligands, a possible ligand set can be proposed. For imidazole and probably imine donors, the ligand's orientation relative to the vanadyl unit can be determined. While this is a valuable method for assessing first coordination sphere ligation to vanadium, careful analysis must be employed. It should be remembered that the solution to the additivity relationship is often not unique. This is because several ligands have similar contributions to $A_{\|}$, the ligand orientation can cause dramatic shifts to $A_{\|}$, and the inherent error of the method is sufficient to make ligands with similar values look identical. For these reasons, other spectroscopic techniques should be used to confirm assignments when the specific ligand types are unknown.

3. Electron-nuclear double resonance (ENDOR)

3.1. Introduction to technique

ENDOR is a powerful tool for the study of complexes containing paramagnetic ions such as VO^{2+}, primarily because inhomogeneous line bordering in conventional EPR spectra often hides hyperfine splittings that arise from ligand nuclei. ENDOR (and ESEEM, cf. Section 4) can sometimes recapture this lost resolution.

In ENDOR spectroscopy, an EPR spectrum is first obtained and the magnetic field set to selected portion of the EPR absorption. Microwave radiation is applied with sufficient power to cause partial saturation of the EPR transitions. Then, with the magnetic field still fixed, ratio frequency energy is applied, and is swept over the range of probable nuclear trasition frequencies. Simulation of such a transition in a coupled nucleus provides a parallel electronic spin relaxation pathway, producing transient relief of the microwave saturation. The subsequent brief increase in the EPR amplitude constitutes an ENDOR signal. ENDOR can thus be thought of as observing NMR by detection of EPR.

The nucleus whose spin transition is detected in the ENDOR experiment is not necessarily the metal nucleus. It can be any nearby nucleus whose spin is coupled to the unpaired electron. ENDOR is generally better suited to the detection of stronger hyperfine couplings, especially in comparison with ESEEM. Fig.

9a shows an example of energy levels for a paramagnetic center with $S = 1/2$, coupled to a nucleus with $I = 1/2$. In ENDOR, the nuclear spin transitions are driven directly, and the transitions represented by the selection rules as $\Delta m_s = 0$, $\Delta m_I = \pm 1$ are, therefore, highlighted (solid arrows). As shown, two lines will be observed, whose transition frequencies are given approximately by:

$$\nu_{ENDOR} = \left| \nu_L \pm \frac{A}{2} \right| \quad (1)$$

where ν_L is the NMR frequency of the nucleus at the applied magnetic field (the Larmor frequency), and A is the hyperfine coupling constant. Thus, if $|A/2| < \nu_L$, the two transitions ν_{ENDOR} are centered about ν_L and separated by A. In the other case ($|A/2| > \nu_L$), the transitions are separated by $2\nu_L$, and $|A|$ is simply $\nu_+ + \nu$. Since, ν_L can be obtained from a table of nuclear properties, the ENDOR data can be used to confirm the identity of the coupled nucleus, as well as the value A at the chosen field. ENDOR linewidths are often measured in tenths of MHz, so that resolution is typically at least two orders of magnitude better than that of CW EPR.

No matter how many equivalent $I = 1/2$ nuclei are present only two transitions will be observed by ENDOR. This represents both an advantage and disadvantage. The total number of spectral lines is obviously reduced, simplifying the spectrum versus CW EPR. However, there is no way to tell from ENDOR how many of each type of nucleus contribute to the spectrum.

The values of ligand hyperfine couplings often exhibit significant anisotropy. For metal cations that have anisotropic EPR spectra, therefore, varying the magnetic field across the resonant EPR absorption (and the resulting changes in the values of A and of ν_L) will cause the spectrum of nuclear transitions to shift. Also, since a single magnetic field setting can encompass a range of orientations, ENDOR spectra are usually more complex in appearance than might be suggested by Eq. (1).

For ^{14}N, with its nuclear spin $I = 1$, the approximate expression for the ENDOR frequencies includes the nuclear quadrupolar interaction, Q:

$$\nu_{ENDOR} = \left| \frac{A}{2} \pm \nu \pm \frac{3Q}{2} \right| \quad (2)$$

As is evident from Fig. 9b, in the absence of a quadrupolar interaction, there will be two nuclear transitions of equal energy for each value of m_s. Since, ^{14}N has small magnetic moment, one will observe, for all but the weakest hyperfine couplings, a pair of lines separated by twice ν_L and centered at $A/2$. The effect of a nonzero quadrupolar coupling is then to split each pair of equivalent transitions, yielding a four-line spectrum. An example is shown in Fig. 10, along with an illustration of the effect of orientation selection on ^{14}N-ENDOR in complex containing VO^{2+}. A more detailed quantum mechanical explanation of ENDOR can be found in a review by Piekara-Sady and Kispert [48].

Pulsed, or electron spin echo ENDOR (ESE-ENDOR) is an advanced form of the ENDOR technique that has come into much greater use in the past decade. In ESE-ENDOR, nuclear spin transitions are detected by their effect on the amplitude of a transient EPR signal called an electron spin echo (see Section 4.1, below) not by their effect on a CW EPR absorption. ESE-ENDOR has advantages in sensitivity over CW ENDOR in many situations, and it usually works over a wider range of temperatures, although, the instrumentation for the pulsed technique is somewhat more complex. A detailed and highly readable description of ESE-ENDOR can be found in the article by Thomann and Bernardo [49].

3.2. Model complexes

Grant and co-workers used ESE-ENDOR to obtain the ^{51}V nuclear quadrupolar coupling constant, $P_{\|}$, and discovered that while it is relatively insensitive to ligands in the equatorial plane, it does change with different axial ligation [50]. Changing equatorial ligands from octaethylporphyrin (oep) to acetylacetonate (acac) to *N*,*N*′-ethylenebis(salicylideneamine) (salen) in complexes with no axial ligands did not significantly alter the $P_{\|}$ from -0.430 MHz. Addition of an axial ligand brought $P_{\|}$ closer to zero, with more donating ligands having a larger effect (Table 2). Interestingly, the placement of imidazole, as an axial ligand only changed $P_{\|}$ to -0.40 MHz. This weak binding and small amount of donation can be explained using the imidazole ring

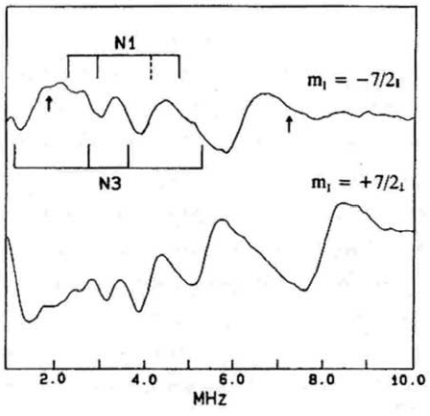

Fig. 10. ^{14}N-ENDOR spectra of vanadyl apo-ferritin observed at the $m_I = -7/2$ parallel line (top) and the $m_I = +7/2$ perpendicular line (bottom) of the EPR spectrum. Reprinted with permission from [54]. Copyright 1991 American Chemical Society.

Table 2
Parallel nuclear quadrupolar coupling constants ($P_{\|}$) observed with different axial ligands

Axial ligand	$P_{\|}$ (MHz)
None[a,b,c]	−0.43
Imidazole[a]	−0.40
Pyridine[c]	−0.369
Ethanol[b]	−0.250
n-Butylamine[a]	−0.24
DMSO[b]	−0.224
Pyridine (acac oxygen)[b]	−0.110

All values from reference [50].
[a] Equatorial ligand: (oep).
[b] Equatorial ligand: (acac).
[c] Equatorial ligand: (salen).

orientation discussion from the EPR section (vide supra). In the axial position, the coordinating nitrogen's aromatic p orbital would be placed in a position to overlap with the vanadium d_{xz} and d_{yz} orbitals, which are already involved in bonding to the vanadyl oxo. The extreme effect of pyridine compared with *n*-butyl amine is explained by its tendency to coordinate in the equatorial plane and displace one of the acac oxygens to the axial position. The expected smaller value for an axial pyridine ligand is observed for VO(salen). It is noted that making ESE-ENDOR measurements on the strongly coupled ^{51}V nucleus required extension of the radio frequency sweep to nearly 300 MHz, well above the standard range for X-band instruments.

The computation of $P_{\|}$ from EPR spectra of the pentaaquo vanadyl cation ($[VO(H_2O)_5]^{2+}$) has been confirmed by density functional theory (DFT) calculations [51]. The theoretical work in this study was checked against the results of EPR measurements performed at both 9 and 94 GHz, as well as ESE-ENDOR at 10 GHz. The agreement with the DFT calculations was excellent. The use of a second microwave frequency (94 GHz) that was far removed from X-band (9–10 GHz) lent confidence to the simulations of the experimental EPR data. It was also determined in this study, that while second-order perturbation calculations of simulated ENDOR spectra were adequate for determining trends in $P_{\|}$, a full matrix diagonalization procedure was preferred for absolute determination of ^{51}V quadrupolar couplings.

In a separate study, Grant et al. found that $P_{\|}$ is also increased by distortion of square pyramidal complexes toward trigonal bipyramidal ones [52]. As the ligand approached an orientation that was *trans* to the oxo, $P_{\|}$ became closer to zero. This result is in agreement with the previous work [50], and further lends support to the conclusion that electron donation in the *trans* position decreases the magnitude of the nuclear quadrupole-coupling constant.

Branca, Micera, and Dessi used ^{1}H-ENDOR to determine the environment of protons near to the vanadium in vanadyl salicylate and phenolate complexes. This in turn allowed for determination of the type of oxygen donor to the vanadium. Protons located alpha to coordinated phenolate groups gave coupling constants of 1.70 MHz, and protons alpha to coordinated aryl carboxylates gave a coupling constant of 0.95 MHz. Thus, these two types of ligands can be distinguished [53].

3.3. Biological systems

The first ENDOR study of a vanadyl-substituted protein was by Hanna, Chasteen, Rottman, and Aisen observing horse spleen apoferritin [54]. Both ^{14}N- and ^{1}H-ENDOR were observed. For additional comparison, ENDOR spectra of vanadyl-substituted transferrin were also observed, as its nitrogen donor was known to be a single imidazole. Mulks and co-workers had previously claimed that both nitrogens of a coordinated imidazole ring contribute to ^{14}N-ENDOR [55], and due to quadrupolar coupling each nitrogen atom produces four $\Delta M_I = \pm 1$ transitions in ENDOR. Therefore, eight lines per inequivalent imidazole were expected for the vanadyl-substituted apoferritin. Although, it was difficult to observe all eight lines (Fig. 12), more than four resonances were found. The assignments shown were tentative, and it was not possible at the time to determine by ENDOR whether one or two nitrogen-containing ligands contributed to the spectra. Later ESEEM work on model complexes by Dikanov et al. showed that in fact the hyperfine couplings to the coordinating and non-coordinating nitrogens differ by more than an order of magnitude (vide infra) [71]. Thus, only a single large hyperfine coupling per imidazole should be observed, suggesting the presence of a second imidazole ligand. The computed hyperfine coupling was 7.14 MHz, similar to the 7.5 MHz for transferrin, but different from the values for coordinated amines (ca. 5 MHz) [56]. ^{1}H-ENDOR showed two pairs of lines from two types of nearby hydrogens. One pair of lines, with a coupling of 1 MHz, disappeared with D_2O exchange. This finding and the 2.02 MHz coupling represented by the remaining two lines is consistent with previous findings for imidazole ligands [55]. This allowed for confirmation of an imidazole ring at the metal binding site. It also showed that while the binding site is accessible to solvent, there is no water directly bound to the metal.

Mustafi and Nakagawa have used EPR and ENDOR to study vanadyl-substituted nephrocalcin, which prevents calcium oxalate crystals from growing to form kidney stones. Circular dichroism spectroscopy verified that there were no extreme changes in the protein folding, although, the presence of charge transfer bands

with the vanadium precluded a precise analysis [57]. ^{1}H-ENDOR of the vanadyl complex with nephrocalcin fraction A (NC-A) showed several peaks, but none at the frequencies observed for waters coordinated to vanadium in $[VO(H_2O)_5]^{2+}$. These peaks also did not disappear in samples run in D_2O, so it was concluded that they were from non-exchangeable protons on nearby residues. Lack of water coordination is rare for calcium–protein systems [58]. ^{14}N-ENDOR data were not shown, but it was stated that no peaks due to imidazole were observed. Since nephrocalcin is rich in aspartate and glutamate residues, a coordination sphere composed entirely of carboxylates was postulated. The $A_{\|}$ values from the EPR are inconsistent with this interpretation. The reported value for the vanadyl–nephrocalcin A complex was $A_{\|} = 535.4$ MHz $= 178.6 \times 10^{-4}$ cm^{-1}. From the additivity values in Table 1, a vanadyl with four carboxylates in the equatorial plane should have an $A_{\|} = 170.8 \times 10^{-4}$ cm^{-1}. Very few ligands contribute more than carboxylate, and those that would be found in the protein are water and perpendicular imidazole, both of which were excluded by ENDOR. Further study will be needed to reconcile the differing conclusions from the two techniques.

Later studies on vanadyl-substituted nephrocalcin fraction C (NC–C) showed a different binding mode for that fraction [59]. The $A_{\|}$ from EPR measurements (539.0 MHz $= 179.7 \times 10^{-4}$ cm^{-1}) in this case is consistent with an equatorial ligand set of three waters and a carboxylate ($A_{\|} = 179.8 \times 10^{-4}$ cm^{-1}) or two waters and two carboxylates ($A_{\|} = 176.8 \times 10^{-4}$ cm^{-1}). ^{1}H-ENDOR spectral comparison with $[VO(H_2O)_5]^{2+}$ indicated water coordination by two different types of protons, the peaks disappeared when the sample was run in D_2O. This leads to the conclusion, that the two water, two carboxylates ligand set is correct. In this case the ENDOR and EPR are complementary, as the ENDOR spectrum can eliminate possibilities that are distinguishable within the error of the EPR activity relationship.

ENDOR particularly as applied to ^{1}H and ^{31}P hyperfine couplings, has proven to be of particular value for structural analysis of vanadyl–nucleotide complexes. Mustafi, et al. used this approach to examine complexes of the form VO(nucleotide)$_2$, where the nucleotide was ADP, ATP, or the α, β-methylene analog of ADP (AMP-CP) [60]. Principal values of proton hyperfine couplings were measured and assigned to solvent, to the ribose or adenine moieties, or to the methylene group of AMP-CP. Distances and angles extracted from these tensors were used as constraints for molecular models of the complexes. Structural parameters for the VO(nucleotide)$_2$ complexes thus obtained proved to be quite similar to those obtained crystallographically for similar complexes formed with other divalent metal cations. The results of this study were later applied to the interpretation of ENDOR spectra of VO^{2+}-GTP and VO^{2+}-GMPPNP complexes bound to the protein elongation factor Tu (EF-Tu). Preliminary ^{1}H-ENDOR measurements, obtained from the $-3/2_{\perp}$ EPR transition, yielded essentially identical spectra for the two complexes, indicating that their active site structures are isomorphous. ENDOR also revealed the presence of at least seven different ^{1}H hyperfine couplings. While these were mostly unassigned, preparation of the protein in denaturated water (and comparison with model studies) allowed attribution of a 3.2 MHz coupling to an axially coordinating water molecule. Vanadium–nuclear distances were calculated for each coupling, apparently by assuming the absence of an isotropic component to the coupling tensor.

3.4. Summary of ENDOR capabilities

What can be determined through the use of ENDOR, greatly depends on which nucleus is being observed. For ^{51}V-ENDOR, the quadrupolar coupling constant, $P_{\|}$, is sensitive to ligation in the axial position. This allows for identification of the axial ligand in terms of its electron-donating ability. ^{14}N-ENDOR can distinguish between coordinated imidazoles and amines by the hyperfine and quadrupolar couplings derived from their nuclear transition frequencies. ^{1}H-ENDOR spectra can be compared with that of $[VO(H_2O)_5]^{2+}$ to identify ligated water. D_2O exchange will remove peaks from exchangeable protons in the area. The coupling constants for nearby protons on alpha carbons of imidazole, phenolate, and salicylate ligands are known.

4. Electron spin echo envelope modulation (ESEEM)

4.1. Introduction to technique

ESEEM is a specialized, pulsed EPR technique, that is used to detect weak nuclear hyperfine couplings. As its name suggests, ESEEM relies upon the generation of electron spin echoes. In pulsed EPR techniques, a series of short, intense microwave pulses, followed by an extended waiting period, replaces continuous microwave irradiation. Application of two microwave pulses to an EPR sample, immersed in a magnetic field at resonance, results in the emission by the sample of a weak, transient microwave signal (Fig. 11a). This signal is the electron spin echo. If the two pulses are separated by a delay time τ, then the echo occurs at time after 2τ after the first pulse. As τ increases, the amplitude of the spin echo decreases roughly exponentially, with a time constant that is strongly temperature-dependant. In biological systems, two-pulse electron spin echoes often fall below the level of detectability for delays (τ) of a

few microseconds or more, even at temperatures near the boiling point (b.p.) of the liquid helium. The decay of the echo as a function of the time before the pulses is slower when three microwave pulses are applied instead of two (Fig. 11b). The three-pulse sequence generates several spin echoes, but the one of the most interest for ESEEM measurements is the 'stimulated echo' that occurs at time τ after pulse III. Here τ is identified as the (fixed) time between pulses I and II. As the delay T between pulses II and III is lengthened, the stimulated echo also decays, but it does so approximately an order of magnitude more slowly than the two-pulse 'primary echo'.

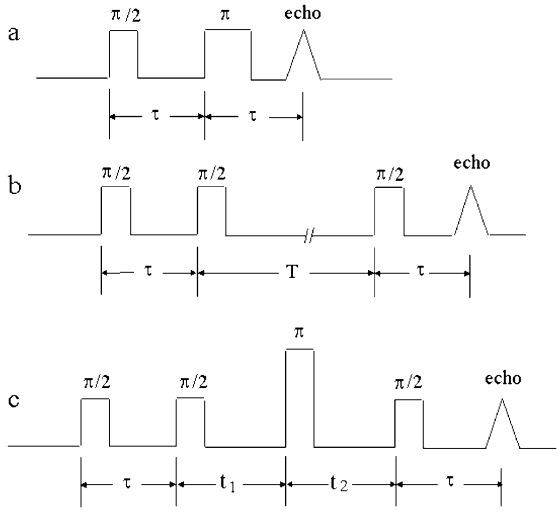

Fig. 11. Microwave pulse sequence for (a) primary ESSEM; (b) stimulated echo ESEEM; and (c) HYSCORE. Sequence (c) can also be used for one-dimensional, four-pulse ESEEM if t_1 and t_2 are varied together.

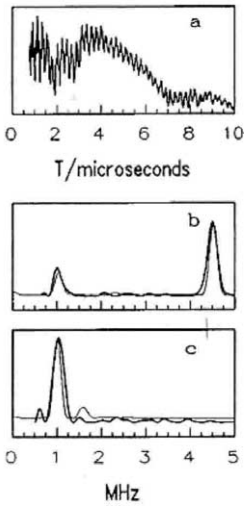

Fig. 12. (a) Time domain, three-pulse (stimulated echo) ESEEM spectrum of $VO(H_2O)$(ada) obtained at the $m_I = +5/2$ perpendicular transition of the vanadyl EPR spectrum. (b) Frequency domain spectrum obtained by Fourier transformation of (a). (c) Frequency domain spectrum at the $m_I = -7/2$ parallel transition. Reprinted with permission from [64]. Copyright 1998 American Chemical Society.

If the unpaired electron is weakly coupled to a nucleus with spin $I > 0$, the spin echo will, in general, decay non-monotonically as a function of the variable delay. This is illustrated in Fig. 12a for the case of a three-pulse experiment. The hyperfine coupling causes the spin echo to be 'modulated', that is, its integrated amplitude decreases periodically (as a function of T) from the value that it would have in the case of no nuclear couplings. ESEEM spectra are often modulated at more than one frequency, and the frequencies are most easily visualized by calculation of the Fourier transform (Fig. 12b) of the modulation function. The plot of the Fourier transform is a frequency-domain spectrum (very similar to an ENDOR spectrum), whose peak positions represent the spin transition energies of hyperfine-coupled nuclei. These energies can be used to determine hyperfine coupling constants as described below. As in ENDOR (vide supra), the spectrum of transitions will shift due to changes in both A and ν_L, as the magnetic field is varied. This is seen in the comparison of Fig. 12 a and c, which were obtained from the same sample. In Fig. 12b, the field was set on a 'perpendicular' transition of a VO^{2+} EPR spectrum, while in Fig. 12c it was set on a 'parallel' transition. Thus, changing the field, effectively changes the subset of sample orientations that is observed, and for the general case of an anisotropic hyperfine coupling, the ESEEM spectrum will change as well.

The intensity of the ESEEM effect (i.e. the depth of the spin echo modulation as a fraction of the total echo intensity) depends upon a number of factors, including the spin of the coupled nucleus. In general, nuclei with spin $I > 1/2$ yield deeper modulations than, those with $I = 1/2$. In the study of vanadyl complexes, ESEEM has found its greatest use in the detection and characterization of ^{14}N ($I = 1$) superhyperfine couplings. While equatorially coordinating ^{14}N produces intense modulations, ^{15}N ($I = 1/2$) yields much weaker modulations (and at different frequencies) in the same chemical environment. This effect can be extremely useful for making definitive identification of the chemical moiety that donates a nitrogen ligand, providing that selective ^{15}N labeling can be accomplished.

Since, ^{14}N has a small nuclear magnetic moment, and because ^{14}N superhyperfine couplings to VO^{2+} are relatively small (< 10 MHz), the ESEEM frequencies arising from such couplings tend to be low. A low-frequency modulation has a long period, and thus, if the echo decays away quickly, it becomes difficult to observe more than a cycle or two of modulation. This translates into broad lines and poor resolution in the frequency-domain spectrum. Therefore, the slower-decaying stimulated echo obtained in the three-pulse ex-

periment generally provides a better resolved ^{14}N:VO^{2+} ESEEM spectrum.

ESEEM spectra are often complicated in appearance, due to orientation selection and to other anisotropic effects. Consequently, theoretical simulation is the best method for extracting hyperfine-coupling tensors from spectral data. Simulations are more credible when one set of parameters fits data obtained at two or more different microwave frequencies. This has motivated a number of workers to construct pulsed EPR spectrometers that operate over a broad frequency range, or at several widely separated frequencies [61,62]. Nevertheless, in many cases, one can make reasonable estimates of superhyperfine coupling constants by direct examination of single-frequency spectra. These estimates are useful as input parameters for initial attempts at spectral simulation. For $I = 1/2$, the nuclear transition frequencies $\nu_{\pm}$ are given by the same approximate expression (Eq. (1)) as for ENDOR.

ESEEM spectra of ^{14}N ($I = 1$), are strongly influenced by the quadrupolar interaction. If the hyperfine coupling and the nuclear Zeeman interaction are similar in magnitude, then the local magnetic fields will cancel for one value of m_s. In that case, the pure nuclear quadrupolar frequencies can be obtained directly from the ESEEM spectrum. These frequencies are represented in two nuclear transitions of the type $\Delta m_I = \pm 1$, plus one of the type $\Delta m_I = \pm 2$ all for the same value of m_s (Fig. 12b). The values of the quadrupole coupling parameters derived from these frequencies are diagnostic of the chemical environment of the ^{14}N nucleus. It is noted that if the microwave frequency (and thus the magnetic resonance field) can be adjusted over a sufficient range, then the aforementioned cancellation of local magnetic fields, which also maximizes the depth of the spin echo modulations, can be brought about at will [63]. This provides further motivation for construction of ESEEM instruments that operate at multiple frequencies.

If, in contrast with the case just considered, the isotropic component of the ^{14}N hyperfine coupling is relatively strong ($A_0 > 5$ MHz), then the two transitions of the type $\Delta m_I = \pm 2$ will generally dominate the ESEEM spectrum. These 'double quantum' transitions occur approximately at frequencies:

$$\nu_{dq\pm} = 2\left[\left(\nu_L \pm \left(\frac{A}{2}\right)\right)^2 + K^2(3+\eta^2)\right]^{1/2} \quad (3)$$

where K is the nuclear quadrupole coupling parameter $e^2Qq/4h$, and η is a parameter between 0 and $+1$ that describes the deviation of the quadrupole coupling tensor from axial symmetry [64]. Having assigned and measured the $\Delta m_I = \pm 2$ transitions, one can estimate the hyperfine coupling A for the orientation selected:

$$A \approx \frac{\nu_+^2 - \nu_-^2}{8\nu_L} \quad (4)$$

By comparing the values of A obtained from biological systems with those from well-characterized model complexes, it is possible to distinguish different classes of equatorial nitrogen ligands, for example, histidine versus lysine in proteins [56,74].

Hyperfine Sublevel Correlation (HYSCORE) spectroscopy is a two-dimensional ESEEM-based method, which is used to help to untangle complex ESEEM spectra [65]. In this technique, a π pulse is inserted between the second and third $\pi/2$ pulses of a stimulated echo sequence (Fig. 11c). The time interval t_1, which precedes the π pulse, is scanned through a series of n discrete steps, and the stimulated echo amplitude is monitored, producing a one-dimensional ESEEM trace in the time domain. The interval t_2, which follows the π pulse, is then lengthened by a step that is equal in size to the steps in t_1, and the scan of t_1 is repeated. By making n such steps in t_2, one obtains a complete, $n \times n$ time domain data set. Two-dimensional Fourier transformation then yields a 2D-frequency spectrum, usually displayed as a contour plot (Fig. 13).

The HYSCORE experiment offers a number of advantages over standard, stimulated-echo ESEEM. First, the added π-pulse serves to create correlations between nuclear spin transitions in different electron spin manifolds, designated m_s. These correlations are evident in the 2D frequency spectrum as off-diagonal peaks (cross peaks, or ridges in the case of anisotropic couplings), such as those labeled **1**, **2**, and **3** in Fig. 13. As is clear from comparing the 2D spectrum to the 1D projections onto the axes, HYSCORE's multidimensional approach provides vastly improved resolution. In addition, cross peaks can appear primarily in the $(++)$ or $(+-)$ quadrant, depending upon the relative magnitudes of the hyperfine and nuclear Zeeman interactions (dominant hyperfine interactions produce cross peaks in the $(+-)$ quadrant, and vice versa). Thus the 2D contour plot provides immediate evidence of the range of values into which each hyperfine coupling falls. Third, the shapes of the cross peaks and their orientations with respect to the diagonal of a given quadrant can be analyzed in a straightforward fashion to extract values of the isotropic and anisotropic parts of ligand hyperfine couplings [66]. Separating these two parameters, aids in determination of electronic and chemical structure. Due to these and other useful properties, HYSCORE should prove to be a powerful tool for analysis of vanadyl complexes in biological settings.

4.2. Model complexes

LoBrutto et al. used ESEEM on crystallographically characterized vanadyl model complexes with axial amine ligands (Fig. 12) to determine that the superhy-

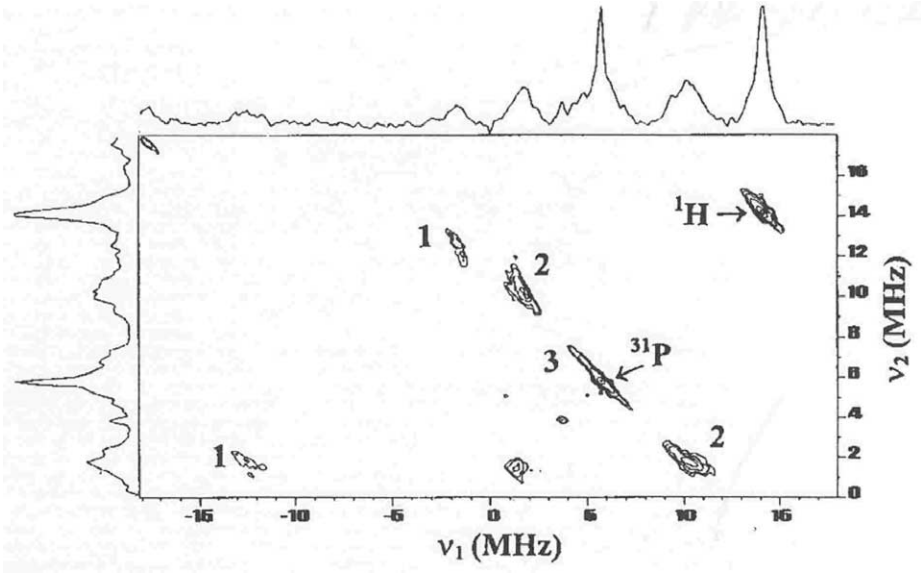

Fig. 13. HYSCORE spectrum of vanadium(IV) in bone measured at the $m_I = -1/2$ line of the vanadyl EPR spectrum. The numbered crosspeaks show the presence of three unique phosphorus nuclei. Reprinted with permission from [82]. Copyright 1999 American Chemical Society.

perfine coupling from an axial amine can be observed. Simulations of the axial nitrogen's three-pulse ESEEM yielded $A_o = 1.3$ MHz. This coupling is much smaller than that attributed to a typical equatorial amine ligand, about 5.0 ± 0.5 MHz. These values supported the conclusion that an axial amine donor is present in the vanadyl-substituted chloroplast F_1-ATPase [64]. Although, the smaller axial superhyperfine coupling was comparable to the smaller coupling observed for the reduced vanadium bromoperoxidase [67], no match was found. It is possible that the rVBrPO coupling at $A_o = 1.8$ MHz could be the result of an axial imidazole donor. This would be true if the change in the equatorial imidazole value ($A_o = 6$–7 MHz) is similar to the factor of four reduction in the amine value when shifted to the axial position.

Fukui and co-workers have shown that ESEEM can distinguish among equatorial amine, imine, and thiocyanate ligands. By matching their spectra to theoretical simulations, these workers determined that the values for the superhyperfine coupling was different in each case. Amines ($A_o = 4.98$–5.10 MHz) were found to have smaller couplings than imines ($A_o = 5.78$–5.83 MHz), which in turn had smaller couplings than thiocyanate ($A_o = 7.47$ MHz) [68]. It is interesting to note that the imine values, obtained from the salen and salophen ligands, are not quite in the range associated with values for imidazole.

Another model complex study by the Fukui group focused on imidazole-containing complexes as possible models for the reduced vanadium bromoperoxidase [69]. ESEEM of VO(Himac)$_2$ showed a single pair of $\Delta m_I = \pm 2$ lines, representing a superhyperfine coupling of equatorial imidazole ligation. The modulation frequencies observed were similar to those seen for rVBrPO [67], and so the presence of two equatorial imidazole ligands to VO in rVBrPO was inferred. EPR model complex work was employed by Smith and co-workers to refine the interpretation of the rVBrPO EPR parameters. The results indicate that such coordination is possible [20], although, the model complex crystal structures contained therein suggest that the imidazoles in VO(Himac)$_2$ may have different orientations to the vanadyl unit than proposed by Fukui. In the same communication, Fukui et al. attempt to distinguish between imine and imidazole coordination in the ESEEM by adding acid to VO(SalimH)(acac) and observing which peaks disappear. Upon addition of acid, two of the four observed peaks completely vanish, confirming that one nitrogen ligand is protonated and no longer bound. Since, the peaks that remained were at the same modulation frequencies as those observed in the ESEEM of VO(Himac)$_2$, it was concluded that the imine had been protonated. As both pairs of peaks represent similar superhyperfine couplings, these couplings cannot distinguish directly between them. However, the previously reported ^{51}V hyperfine coupling constant, re-evaluated in light of the imidazole orientation data, may confirm this conclusion. Upon protonation, the $A_\parallel$ value increases by 4×10^{-4} cm^{-1} [70]. This value is closer to the contribution difference between water and an imine ligand ($\Delta A_\parallel = 5.4 \times 10^{-4}$ cm^{-1}) than the difference between water and the newly established additivity contribution from imidazole ($\Delta A_\parallel = 1.3 \times 10^{-4}$ cm^{-1}).

Recent work by the Fukui group also seeks to distinguish nitrogen donors. The ESEEM of a vanadyl model complex with amidate nitrogen coordination was stud-

ied [71]. Since, the observed superhyperfine coupling is indistinguishable from imidazole ($A_o = 6.7$ MHz), another method of analysis is necessary to distinguish the two. Fukui and co-workers found that the nuclear quadrupolar coupling parameters, e^2Qq/h and η, can distinguish amidate from imidazole. The reported values were, $e^2Qq/h = 2.5$ MHz and $\eta = 0.04$ for the amidate versus $e^2Qq/h = 2.2$ MHz and $\eta = 0.64$ for imidazole [69]. The orientations of the quadrupolar tensor axes with respect to the V–N bond direction, was found to be different for the two classes of compounds [71]. This discovery is potentially applicable to difficulties in distinguishing other types of ligands as well, such as the imine–imidazole case above.

Dikanov and co-workers took advantage of the fact that larger coupling constants (9–10 MHz) from nuclei with spin $I = 1/2$ produce only a very weak ESEEM effect, to determine the coupling from the remote nitrogen of imidazole [72]. ^{15}N-labelled imidazoles was used, and as the couplings for ^{15}N are proportionally larger than for ^{14}N, the hyperfine couplings from the nitrogen directly bonded to the vanadium (6–7 MHz for ^{14}N) were not detected. The only couplings observed for VO(^{15}N-imidazole)$_4$ were small, at values of 0.28–0.57 MHz, which would correspond to ca. 0.3 MHz for ^{14}N. This is lower than the directly bonded nitrogen by a factor of 20, and similar to findings with complexes of other metals. Dikanov has also used isotopic substitution to determine that free histidine will bind in the equatorial plane to vanadyl through both amine and imidazole moieties [73]. HYSCORE was employed in this study to verify the assignment of the myriad of nitrogen peaks present in the ESEEM. In fact, this work stands as a remarkable example of the power of the HYSCORE method, when applied carefully, to sort out extremely complex ESEEM data.

4.3. Biological systems

Zhang and co-workers have used the vanadyl ion as a probe of S-adenosylmethionine synthetase [74]. In this system, vanadyl can be substituted specifically for one of the two native Mg^{2+} cations. Most catalytic activity is retained so long as Mg^{2+} is present in the second site. An equatorial amine donor was observed, with A_o values ranging from 4.3 to 5.4 MHz, in those complexes that contained phosphate in some form (ADP or ATP, or tripolyphosphate). Blanket isotopic substitution of ^{15}N in the enzyme was employed to distinguish whether the amine ligand was from the enzyme (in which case the ESEEM peaks for ^{14}N would disappear, as they in fact did) or from the methionine substrate. With the specific isotopic substitution into lysine, it was determined that the binding amine is from a lysine residue of the enzyme in all cases save the final intermediate. In that case, where no form of phosphate is included in the active site complex, the ESEEM spectrum was unchanged with ^{15}N substitution into the entire protein. Instead, the use of ^{15}N at the α-amino position of the methionine moiety of the product AdoMet showed that that nitrogen was now an equatorial ligand. Thus, ESEEM allowed for the observation of a change in coordination in a manner that cannot be observed with EPR, due to the similarity of the ligands.

Houseman et al. have also used ESEEM to study vanadyl chloroplast F_1-ATPase [75]. Before the confirmation of the axial effect on the superhyperfine coupling, this combined EPR and ESEEM analysis allowed the authors to postulate that an axial amine donor was involved, as the interpretation of the EPR data placed the vanadyl ion in the proper position for a lysine to bind axially. ESEEM data later provided strong support for this assignment, using the model complex study described above.

Dikanov and co-workers used ESEEM to confirm imidazole ligation of vanadyl in the high-affinity binding site of D-xylose isomerase [76]. In this case, vanadyl ion is an inhibitor of the enzyme. In addition to the ^{14}N peaks, these researchers analyzed peaks from ^{1}H modulations, which typically appear above 10 MHz. The large superhyperfine couplings found from the protons confirmed the conclusion, based upon the ^{14}N peak assessment, that the imidazole is indeed coordinated in the equatorial plane. This study is notable for two reasons in addition to its immediate biological significance. First, the employed four-pulse ESEEM to study the proton couplings. This method is one-dimensional version of the HYSCORE sequence, in which $t_1 = t_2$ and in which these two delays are varied together while the stimulated echo is monitored. This yields an ESEEM spectrum that has the additional information content (i.e. sum and difference frequencies) of two-pulse ESEEM, but in which the echo decay is very much slower, yielding enhanced resolution in the frequency domain. Second, usually detailed description is provided for the simulation of a very complex two-pulse ESEEM spectrum of the histidine-based, equatorial nitrogen ligand. This paper should therefore be of considerable use to investigators of similar systems.

Gerfen et al. studied horse apo-ferritin with vanadyl ion added [77]. A competitive binding study was used to determine that vanadyl and Fe^{2+} compete for the same binding site. The ESEEM showed the presence of a nitrogen donor with a large superhyperfine coupling constant of 7.1 MHz, indicative of equatorial imidazole ligation. Upon substituting D_2O as the solvent, a significant amplitude reduction occurred in the proton modulation frequencies, leading to the conclusion that water is also bound in the equatorial plane. Grady et al. have used a combination of site-directed mutagenesis and CW EPR to show that His 118 is the likely source of the ^{14}N ligand to vanadyl, which was previously

detected by ESEEM. His 118 lies on the outer surface of the protein, near the entrance to the three-fold channel. Vanadyl bound at this site is thought to give rise to the so-called 'β' signal in the EPR spectrum [78].

Petersen and co-workers have taken advantage of the ease of nitrogen ligand identification provided by ESEEM to investigate vanadyl-substituted imidazole glycerol phosphate dehydratase. The vanadyl ion in this case is not being used as a substitute for an active site metal, but for divalent cations, which assemble the enzyme into its highest molecular weight form. The presence of an equatorial imidazole ligand was easily established, and poorly resolved peaks at lower modulation frequencies may be the result of a second imidazole, coordinated axially [79].

Buy et al. have used ESEEM and HYSCORE of vanadyl to study the Mg^{2+} binding sites of bacterial TF1-ATPase. The vanadyl-substituted enzyme did retain some activity, but only 12% of that of the Mg-ATPase. Previous EPR studies had established moderately low $A_{\|}$ values implying at least one nitrogen ligand. With multiple nitrogen ligands with a close similarity in modulation frequencies and superhyperfine couplings, the HYSCORE plots were necessary to assign the peaks properly. Two nitrogen ligands were found—an equatorial amine and an equatorial imidazole. ESEEM peaks attributable to ^{31}P were also seen, and were distinct from the nitrogen modulation frequencies observed [80].

Further studies by the Zimmermann group focused on subunits of the TF1-ATPase [81]. Again using both ESEEM and HYSCORE, the α and β subunits were both found to bind vanadyl through an equatorial amine donor. The $\alpha_3\beta_3$ hexameric fragment was, however, similar to the whole enzyme in that superhyperfine couplings attributable to both equatorial amine and imidazole ligands were observed.

A recent collaboration between the Dikanov and Orvig groups used ESEEM and HYSCORE to find vanadium coordinated to phosphate in the bones of diabetic rats fed the vanadyl complex with BEOV [82]. Examination of the HYSCORE cross peaks allowed for the identification of three different environments for ^{31}P atoms near vanadium (Fig. 13). These couplings are similar to those previously reported [47,80]. A weak proton hyperfine coupling was also observed, and was assigned to water or hydroxide completing the coordination sphere.

Fukui et al. have also used ESEEM to study the fate of vanadyl complexes in vivo, starting with vanadium in the form of vanadyl–histidine [83] and vanadyl bis(picolinate) [84]. A survey with EPR and ESEEM showed that in none of the organs observed (kidney, liver, bone) did the complex remain intact. Although, the EPR hyperfine coupling values were close for kidney and liver, the ESEEM showed that the vanadium is actually bound to an amine, not an aromatic imine. Their EPR $A_{\|}$ value for bone (173.5×10^{-4} cm^{-1}) is comparable to Dikanov and Orvig's findings (171×10^{-4} cm^{-1}) [82]. For the ESEEM of bone, no modulation frequencies due to ^{14}N were found, only those from ^{31}P.

4.4. Summary of ESEEM capabilities

ESEEM so far has been most used for, and is best suited towards, identification of nitrogen donors to vanadium. Many different types of nitrogen donors can be distinguished by the superhyperfine coupling. Axial donation can be determined for amines and possibly imidazoles or imines. Even those ligands with similar couplings may be able to be resolved by analysis of quadrupolar couplings. Phosphate donors can be identified by phosphorus modulation frequencies, which can often be distinguished by their dependencies on applied magnetic field. Nearby exchangeable protons can be detected, whether they are from water or from protein based sites, by exchange with denaturated solvent. The presence of coupled, non-exchangeable protons, which can be associated with the protein, substrates, or cofactors, can also be identified by solvent exchange experiments. Further, such couplings can be assigned definitively in cases where specific deuteration (such as by organic synthesis) is feasible. Complicated spectra can be simplified by isotopic nitrogen or hydrogen substitution and correct pairing of peaks can be determined by examining the cross peaks of the two-dimensional, technique HYSCORE. The primary weakness of ESEEM is in identifying oxygen donors, for which other techniques that do not look upon the ligand atom's nuclear spin have to be used.

5. Conclusion

The three spectroscopic techniques discussed, EPR, ESEEM, and ENDOR, are a powerful set of complementary techniques for identifying the surroundings of the vanadyl ion. Although, at the present, none of them is appropriate for all situations, the three combined can, and have, defined the metal binding sites of several complicated systems. In many cases one can substitute the vanadyl ion for spectroscopically silent divalent cations, particularly the biologically important Mg^{2+}, Ca^{2+}, and Zn^{2+}, and this approach will find many more useful applications. A standard procedure is already being developed. EPR is first used to determine a set of possible equatorial ligand environments. Then, ESEEM is used to identify and position nitrogen-containing ligands, as well as to identify nearby exchangeable protons or phosphate ligands. ENDOR will then confirm the nitrogen donors, the exchangeable protons

(and perhaps distinguish oxygen donors alpha to non-exchangeable protons), and identify the presence and type of axial ligand. All three are even being used outside biological systems, several studies of the structures of industrial catalysts have been reported [85]. As these techniques continue to be used, their power to characterize complex sites will undoubtably grow. This is especially true for ENDOR. Even applications of the additivity relationship continues to be refined so as to prove more informative, and newer techniques such as pulsed ENDOR promise to extend the applicability of vanadyl as a biological probe.

Acknowledgements

This work has been supported by the NIH, grant no.: 5R01 GM42703-11 to V.L. Pecoraro.

References

[1] M. Henze, Hoppe-Seyler's Z. Physiol. Chem. 72 (1911) 494.
[2] (a) R.R. Eady, in: R.R. Eady (Ed.), Vanadium Nitrogenases, Kluwer Academic Publishers, Boston, FL, 1990, pp. 99–127; (b) H. Vilter, Phytochemistry 23 (1984) 1387.
[3] F.H. Nielsen, J. Trace Elem. Exp. Med. 13 (2000) 113.
[4] E.L. Tolman, E. Barris, M. Burns, A. Pansisni, R. Partridge, Life Sci. 25 (1979) 1159.
[5] S.S. Eaton, G.R. Eaton, in: N.D. Chasteen (Ed.), Vanadium in Biological Systems, Kluwer, Boston, FL, 1990, pp. 199–219.
[6] M.W. Makinen, D. Mustafi, in: H. Sigel, A. Sigel (Eds.), Metal Ions in Biological Systems, Marcel Dekker, Inc, New York, 1995, pp. 89–127.
[7] N.D. Chasten, in: J.F. Riordan, B.L. Vallee (Eds.), Methods in Enzymology, Academic Press, New York, 1993, 227 (8), pp. 232–244.
[8] E. Bayer, H. Kneifel, Z. Naturforsch. 27b (1972) 207.
[9] R.E. Berry, E.M. Armstrong, R.L. Beddoes, D. Collison, S.N. Ertok, M. Helliwell, C.D. Garner, Angew. Chem. Int. Ed. 38 (1999) 795.
[10] R.S. Drago, Physical Methods for Chemists, HBJ Publishing, Ft. Worth, TX, 1992.
[11] A. Abragam, Electron Paramagnetic Resonance of Transition Metal Ions, Oxford, Clarendon Publishing, New York, 1970.
[12] A. Bencini, D. Gatteschi, in: E.I. Solomon, A.B.P. Lever (Eds.), Inorganic Electronic Structure and Spectroscopy, vol. 1, Wiley, New York, 1999, p. 93.
[13] WINEPR SimFonia v1.25, Bruker Analytische Messtechnik GmbH, 1996.
[14] K. Wuthrich, Helv. Chim. Acta 48 (1965) 1012.
[15] N.D. Chasteen, in: L.J. Berliner, J. Reuben (Eds.), Biological Magnetic Resonance, vol. 3, Plenum Press, New York, 1981, pp. 53–119.
[16] B.H. Hamstra, A.L.P. Houseman, G.J. Colpas, J.W. Kampf, R. LoBrutto, W.D. Frasch, V.L. Pecoraro, Inorg. Chem. 36 (1997) 4866.
[17] Computer Simulation of Powder Spectra. R.L. Belford, M.J. Nilges, EPR Symposium, 21st Rocky Mountain Conference, Denver, CO, 1979.
[18] C.R. Cornman, K.M. Geiser-Bush, S.P. Rowley, P.D. Boyle, Inorg. Chem. 36 (1997) 6401.
[19] C.R. Cornman, E.P. Zovinka, Y.D. Boyajian, K.M. Geiser-Bush, P.D. Boyle, P. Singh, Inorg. Chem. 34 (1995) 4213.
[20] T.S. Smith, C.A. Root, J.W. Kampf, P.G. Rasmussen, V.L. Pecoraro, J. Am. Chem. Soc. 122 (2000) 767.
[21] R.J. DeKoch, D.J. West, J.C. Cannon, N.D. Chasteen, Biochemistry 13 (1974) 4347.
[22] D.C. Rees, M. Lewis, W.N. Lipscomb, J. Mol. Biol. 168 (1983) 367.
[23] E. de Boer, K. Boon, R. Wever, Biochemistry 27 (1988) 1629.
[24] M. Weyand, H.J. Hecht, M. Kiess, M.F. Liaud, H. Vilter, D. Schomburg, J. Mol. Biol. 293 (1999) 595.
[25] A.J. Tasiopoulos, A.N. Troganis, A. Evangelou, C.P. Raptopoulou, A. Terzis, Y. Deligiannakis, T.A. Kabanos, Chem. Eur. J. 5 (3) (1999) 910.
[26] H. Hagen, A. Barbon, E.E. van Faassen, B.T.G. Lutz, J. Boersma, A.L. Spek, G. van Koten, Inorg. Chem. 38 (1999) 4079.
[27] S. Mondal, P. Ghosh, A. Chakravorty, Inorg. Chem. 36 (1997) 59.
[28] J.C. Pessoa, I. Cavaco, I. Correia, M.T. Duarte, R.D. Gillard, R.T. Henriques, F.J. Higes, C. Madeira, I. Tomaz, Inorg. Chim. Acta 293 (1) (1999) 1.
[29] H. Sakurai, H. Watanabe, H. Tamura, H. Yasui, R. Matsushita, J. Takada, Inorg. Chim. Acta 283 (1998) 175.
[30] F.C.S. de Paula, S. Carvalho, H.A. Duarte, E.B. Paniago, A.S. Mangrich, E.C. Pereira-Maia, J. Inorg. Biochem. 76 (1999) 221.
[31] R.P. Ferrari, E. Laurenti, S. Poli, L. Casella, J. Inorg. Biochem. 45 (1992) 21.
[32] S.S. Amin, K. Cryer, B. Zhang, S.K. Dutta, S.S. Eaton, O.P. Anderson, S.M. Miller, B.A. Reul, S.M. Brichard, D.C. Crans, Inorg. Chem. 39 (2000) 406.
[33] M. Velayutham, B. Varghese, S. Subramanian, Inorg. Chem. 37 (1998) 1336.
[34] A. Dessi, G. Micera, D. Sanna, J. Inorg. Biochem. 52 (1993) 275.
[35] F.S. Jiang, M.W. Makinen, Inorg. Chem. 34 (1995) 1736.
[36] G. Micera, A. Dessi, D. Sanna, Inorg. Chem. 35 (1996) 6349.
[37] B.G. Werneberg, D.E. Ash, Biochemistry 36 (1997) 14392.
[38] (a) N.F. Albanese, N.D. Chasteen, J. Phys. Chem. 82 (1978) 910; (b) G.D. Markham, Biochemistry 23 (1984) 470.
[39] (a) K.A. Lord, G.H. Reed, Inorg. Chem. 26 (1987) 1464; (b) G.D. Markham, T.S. Leyh, J. Am. Chem. Soc. 109 (1987) 599.
[40] G.R. Hanson, Y. Sun, C. Orvig, Inorg. Chem. 35 (1996) 6507.
[41] C.-Y. Hu, A.L.P. Houseman, L. Morgan, A.N. Webber, W.D. Frasch, Biochemistry 35 (1996) 12201.
[42] W. Chen, R. LoBrutto, W.D. Frasch, J. Biol. Chem. 274 (1999) 7089.
[43] C.-Y. Hu, W. Chen, W.D. Frasch, J. Biol. Chem. 274 (1999) 30481.
[44] E. Kiss, E. Garribba, G. Micera, T. Kiss, H. Sakurai, J. Inorg. Biochem. 78 (2000) 97.
[45] D. Sanna, I. Bodi, S. Bouhsina, G. Micera, T. Kiss, J. Chem Soc. Dalton Trans. (1999) 3275.
[46] D. Sanna, G. Micera, P. Buglyo, T. Kiss, T. Gajda, P. Surdy, Inorg. Chim. Acta 268 (1998) 297.
[47] A.S. Ceccato, A. Neves, M.A. de Brito, S.M. Drechsel, A.S. Mangrich, R. Werner, W. Haase, A.J. Bortoluzzi, J. Chem. Soc. Dalton Trans. (2000) 1573.
[48] L. Piekara-Sady, L.D. Kispert, in: C.P. Poole, H.A. Farach (Eds.), Handbook of Electron Spin Resonance, AIP Press, New York, 1994, pp. 312–356.
[49] H. Thomann, M. Bernardo, in: L.J. Berliner, J. Reuben (Eds.), Biological Magnetic Resonance, vol. 13, Plenum Press, New York, 1993, pp. 275–322.
[50] C.V. Grant, J.A. Ball, B.J. Hamstra, V.L. Pecoraro, R.D. Britt, J. Phys. Chem. B 102 (1998) 8145.

[51] C.V. Grant, W. Cope, J.A. Ball, G.G. Maresch, B.J. Gaffney, W. Fink, R.D. Britt, J. Phys. Chem. B 103 (1999) 10627.
[52] C.V. Grant, K.M. Geiser-Bush, C.R. Cornman, R.D. Britt, Inorg. Chem. 38 (1999) 6285.
[53] M. Branca, G. Micera, A. Dessi, J. Chem. Soc. Dalton Trans. (1990) 457.
[54] P.M. Hanna, N.D. Chasteen, G.A. Rottman, P. Aisen, Biochemistry 30 (1991) 9210.
[55] C.F. Mulks, B. Kirste, H. van Willigen, J. Am. Chem. Soc. 104 (1982) 5906.
[56] P.A. Tipton, J. McCracken, J.B. Cornelius, Biochemistry 28 (1989) 5720.
[57] D. Mustafi, Y. Nakagawa, Proc. Natl. Acad. Sci. USA 91 (1994) 11323.
[58] J. Glusker, Adv. Protein Chem. 42 (1991) 1.
[59] D. Mustafi, Y. Nakagawa, Biochemistry 35 (1996) 14703.
[60] D. Mustafi, J. Telser, M.W. Makinen, J. Am. Chem. Soc. 114 (1992) 6219.
[61] H.L. Flanagan, G.J. Gerfen, D.J. Singel, J. Chem. Phys. 88 (1998) 20.
[62] D.J. Singel, in: A.J. Hoff (Ed.), Advanced EPR. Applications in Biology and Biochemistry, Elsevier, Amsterdam, 1989, pp. 119–133.
[63] A. Lai, H.L. Flanagan, D.J. Singel, J. Chem. Phys. 89 (12) (1988) 7161.
[64] R. LoBrutto, B.J. Hamstra, G.J. Colpas, V.L. Pecoraro, W.D. Frasch, J. Am. Chem. Soc. 120 (1998) 4410.
[65] P. Hofer, A. Grupp, H. Nebenfuhr, M. Mehring, Chem. Phys. Lett. 132 (3) (1986) 279.
[66] S.A. Dikanov, M.K. Bowman, J. Mag. Reson. A 116 (1995) 125.
[67] E. de Boer, C.P. Keijzers, A.A.K. Klaassen, E.J. Reijerse, D. Collison, C.D. Garner, R. Wever, FEBS Lett. 235 (1998) 93.
[68] K. Fukui, H. Ohya-Nishiguchi, H. Kamada, Inorg. Chem. 36 (1997) 5518.
[69] K. Fukui, H. Ohya-Nishiguchi, H. Kamada, Inorg. Chem. 37 (1998) 2326.
[70] C.R. Cornman, J.W. Kampf, M.S. Lah, V.L. Pecoraro, Inorg. Chem. 31 (1992) 2035.
[71] K. Fukui, H. Fujii, H. Ohya-Nishiguchi, H. Kamada, Chem. Lett. (2000) 198.
[72] S.A. Dikanov, C. Burgard, J. Huttermann, Chem. Phys. Lett. 212 (1993) 493.
[73] S.A. Dikanov, R.I. Samoilova, J.A. Smieja, M.K. Bowman, J. Am. Chem. Soc. 117 (1995) 10579.
[74] C. Zhang, G.D. Markham, R. LoBrutto, Biochemistry 32 (1993) 9866.
[75] A.L.P. Houseman, R. LoBrutto, W.D. Frasch, Biochemistry 34 (1995) 3277.
[76] S.A. Dikanov, A.M. Tyryshkin, J. Huttermann, R. Bogumil, H. Witzel, J. Am. Chem. Soc. 117 (1995) 4976.
[77] G.J. Gerfen, P.M. Hanna, N.D. Chasteen, D.J. Singel, J. Am. Chem. Soc. 113 (1991) 9513.
[78] J.K. Grandy, J.L. Shao, P. Arosio, P. Santambrogio, N.D. Chasten, J. Inorg. Biochem. 80 (2000) 107.
[79] J. Petersen, T.R. Hawkes, D.J. Lowe, J. Am. Chem. Soc. 120 (1998) 10978.
[80] C. Buy, T. Matsui, S. Andrianambinintsoa, C. Sigalat, G. Girault, J.-L. Zimmermann, Biochemistry 35 (1996) 14281.
[81] J.-L. Zimmermann, T. Amano, C. Sigalat, Biochemistry 38 (1999) 15343.
[82] S.A. Dikanov, B.D. Liboiron, K.H. Thompson, E. Vera, V.G. Yuen, J.H. McNeill, C. Orvig, J. Am. Chem. Soc. 121 (1999) 11004.
[83] K. Fukui, H. Ohya-Nishiguchi, M. Nakai, H. Sakurai, H. Kamada, FEBS Lett. 368 (1995) 31.
[84] K. Fukui, Y. Fujisawa, H. Ohya-Nishiguchi, H. Kamada, H. Sakurai, J. Inorg. Biochem. 77 (1999) 215.
[85] A. Togni, G. Rist, G. Ribs, A. Schweiger, J. Am. Chem. Soc. 115 (1993) 1908.